A comparative study on silicon-based negatrode materials in metallic cavity electrode and button half cell --- Uncovering unseen microscopic and dynamic features

Yu Tan[1], Qilun Xiong[1], Tingting Jiang[1,*], Fangqi Tang[1], Yingke Zhou[1,*], George Z. Chen[2,*]

1 The State Key Laboratory of Refractories and Metallurgy, College of Materials and Metallurgy, Institute of Advanced Materials and Nanotechnology, Wuhan University of Science and Technology, Wuhan 430081, P. R. China.
2 Department of Chemical and Environmental Engineering, Faculty of Engineering, University of Nottingham, Nottingham NG7 2RD, U.K.

* Email: ttjiang@wust.edu.cn (T. Jiang), zhouyk@wust.edu.cn (Y. Zhou), and george.chen@nottingham.ac.uk (G. Z. Chen)

Abstract

The electrochemical characterization of lithium storage materials using the button cell is commonplace, but it is also tedious and time-consuming. Also, the results are often affected by the use of the binders and separator membranes, and by the electrode forming and cell assembly methods. To study the changes in materials before and after dis-/charging, one has to break up the button cell and disturb the packing structure of electrode. In this work, the metallic cavity electrode made of copper (Cu-MCE) was used to study silicon-based negative electrode (negatrode) materials during electrochemical de-/lithiation. The initial apparent reaction area (i.e. the contacting area between the Cu substrate and the active materials, 0.785 mm^2) of the Cu-MCE was much smaller than that of the half-button cell (153.86 mm^2), reducing significantly the overall current and hence polarization in the Cu-MCE. Powders of commercial silicon and phosphorus-doped silicon (P-doped Si) were tested in the Cu-MCE and a conventional button cell. Cyclic voltammograms (CVs) recorded using the Cu-MCE showed full activation in the first cycle, unlike the button cell whose CVs expanded continuously beyond five cycles. Current peaks on the CVs of the Cu-MCE agreed with the expected redox reactions but were more pronounced. The subtle differences between P-doped Si and pure Si could also be revealed by the Cu-MCE with the current peaks becoming more obvious, apparently due to modification in material structures and improved ion transport dynamics. The peak currents on the CVs of the Cu-MCE were plotted against the square root of scan rate ($v^{1/2}$), showing non-linearity for the two oxidation peaks at 0.35 and 0.54 V, indicating both diffusion and surface of the delithiation processes. Linear plots were obtained for the two reduction peaks at 0.165 and 0.245 V with comparable slopes (-0.024 and 0.029 $mA/(mV/s)^{1/2}$), confirming diffusion control with insignificant polarization. However, similar analyses of the button cell revealed diffusion control in both oxidation and reduction, indicating slower dynamics with large polarization to delithiation. More importantly, the Cu-MCE can be inspected directly after dis-/charging without any disturbance, and provides unseen variation in the packing structure, particle morphology, and elemental information of the active materials. It is hoped that the higher accuracy, better details, and greater efficiency offered by the Cu-MCE for studying the intrinsic electrode reaction characteristics of Si-based electrode materials can be extended to other powdery materials for charge storage.

***Keywords*: Metallic cavity electrode; Microscopic analysis; Dynamic behavior; Silicon negative electrode; Lithium ion batteries**

Introduction

Renewable energy technologies are urgently needed to avoid the fact-based prediction of the detrimental impact on climate and the environment from the unsustainable use of fossil fuels. However, solar and wind sources are featured by their intermittent availability and hence inability to continuously output stable electricity, which challenges their connection to the power grid. At present, a practically achievable solution is to couple renewable energy sources with appropriate energy storage and conversion technologies (ESCTs).

As one of the representatives of ESCTs, lithium-ion batteries (LIBs) are widely used for energy storage due to their wide voltage window, high energy efficiency, low self-discharge rate, and manageable environmental impact. However, the current LIBs are still unable to meet the requirements for large specific charge and energy capacities (> 700 mAh g^{-1} and > 500 Wh kg^{-1}), long cycle life (>5000 cycles), and high power capability (> 5 kW kg^{-1}). Improving the existing and developing new electrode materials are amongst the highly focused research efforts in recent years.

Graphite dominates the present industrial negative electrode (negatrode, which is used to replace the incorrectly used term “anode” in many rechargeable battery literatures because any electrode can be an anode or cathode depending its charging or discharging status) materials, but its capacity (372 mAh g^{-1}) is unsatisfactory.[1, 2] Silicon (Si) and Si-based materials with a higher specific capacity and a potential close to that of the Li/Li^+ couple [2-5] are very promising candidates for negatrode materials. Besides, silicon also has the advantages of high abundance in the earth’s crust, low cost, and environmental friendliness. However, silicon-based negatrode materials suffer from a huge volume variation during lithiation and delithiation, and low carrier diffusion rates. As a result, the capacity and electrochemical performance degrade quickly due to the pulverization and structural collapse of silicon. The formation of the solid electrolyte interphase (SEI) consumes Li^+, resulting in poor initial charge efficiency. There have been many attempts to overcome these obstacles.[6] Designing nanostructures and combination with other materials such as metals, oxides, and carbon can bring about improved stability and rate capability for silicon-based materials.[7, 8] However, a comprehensive understanding of the mechanism of the de-/lithiation of silicon has not yet been confirmed and agreed upon. At the same time, the formation and quality of the SEI, which plays an important role in the performance of the negatrode, also depend on the type and composition of the electrolyte.[7] The selection and use of available electrolyte permeable separator membranes, conducting additives and binders for powders of Si based materials, and the fabrication method for the button type half and full cells will all impact the final performance characteristics of the electrode materials. The procedures for these testing are tedious and time consuming.[9] Therefore, a quicker and more convenient approach without compromising the detail and accuracy is desirable to replace or at least to complement the widely used button cell testing protocols.

The metallic cavity electrode (MCE) shows the advantages of no or little effects from ion diffusion, electrode resistance and double-layer capacitance. It offers a fast and efficient

electrochemical analysis of powdery materials in microgram quantities, and has a wide application spectrum, such as performance comparison between functional and energy storage materials, biological targets assessment, activity ranking of catalysts, and identification of corrosion mechanisms.[10-17] In micro-analysis, such as biological probe and electron microscope loading probe, high-quality clear images could be obtained due to the good charge conduction property of the MCE which facilitates electron conduction through the contact between the MCE and material particles. In molten salt electrolysis and catalytic reaction, the redox-active material in the MCE forms a unique electrochemical environment, giving rise to the featured electrochemical behavior with low polarization.[10, 11, 18-20]

In this work, the MCE was for the first time fabricated by mechanically drilling a circular hole (the cavity) through a thin copper (Cu) foil and applied to characterize Si-based negatrode materials. In comparison with the conventional button half cell, the Cu-MCE offers more convenient operation and reduced testing times without the influence of the binder and separator. It also enables a direct study on the electrochemical reaction mechanism during dis-/charging. Cyclic voltammograms (CVs) of several Si-based negatrode materials were studied in both the Cu-MCE and button half-cells. The results have successfully proven the Cu-MCE to be a convenient, quick and reliable tool for the electrochemical analysis of Si-based negatrode materials. It could also be a promising and generic tool for investigating the reaction natures of other electrode materials quickly and conveniently. It should be stated that although the Cu-MCE has been designed to be used alone, it can also function as a good complement to the button cell in the laboratory, particularly facilitating analyses after various electrochemical tests.

Experimental Section

Materials

Si powder (ca. 200 nm in particle size, Shanghai Naiou Co., Ltd.), phosphoric acid (Shanghai Aladdin Biochemical Technology Co., Ltd. AR, 85%, ρ = 1.685 g mL^{-1}), and ethanol (Sinopharm Chemical Reagent Co., Ltd. AR, 99.7%, ρ (20 ºC) = 0.789 g mL^{-1}) were used as received. To make P-doped Si, the Si powder (1 g) was added into 340 μL phosphoric acid, followed by mixing with ethanol ($\leq$ 5 mL) under stirring for 10 min to produce a uniform slurry which was then placed in an oven at 80 ºC for 5 h to remove ethanol. The drying led to powdery samples which were annealed in quartz boats at 900 ºC for 4 h in Ar to form phosphorus-doped Si powders.

MCE and button cell fabrication

MCE: A copper (Cu) foil (length: 75 mm, width: 2 mm, thickness: 0.5 mm) was used to fabricate the Cu-MCE. The diameter of the mechanically drilled circular through hole (i.e. cavity) was 0.5 mm. A Cu wire (diameter 2 mm) was used to wrap a lithium (Li) disc (diameter: 14 mm, thickness: 1 mm) as the counter and reference dual-electrode. The surfaces of the Cu-MCE and Cu wire were ground on 800-mesh sandpaper and cleaned ultrasonically briefly in hydrochloric acid (to remove surface oxide), ethanol, and deionized water 2 to 3 times. Finally, the electrodes were dried under a vacuum for 5 to 8 min. The Si and P-doped Si powders were each ground with the carbon black Super P® as a conductive agent at a mass ratio of 7:3 for 20 min. These powder mixtures were each filled in the Cu-MCE by pressing its hole repeatedly

on a small pile of the powder. Afterwards, the surfaces of the filled Cu-MCE were wiped using a piece of cloth to remove any excess powders. The loaded Cu-MCE (working electrode) and the Li disc (counter and reference dual-electrode) were inserted into a sealable vase which was then filled with the electrolyte in a glove box under argon. The electrolyte was prepared by adding $LiPF_6$ (1 mol L^{-1}) into a 1:1 (vol: vol) mixture of ethylene carbonate (EC) and dimethyl carbonate (DMC) with fluoroethylene carbonate (FEC, 10 %) as an additive. The electrolyte was kept in the glove box for 4-5 hours before use.

Button cell (also known as coin cell): The Si and P-doped S powders, Super P, and carboxymethylated cellulose (binder) were mixed in the mass ratio of 7:1.5:1.5 (total mass = 0.85 mg). This mixture was ground for 20 min, then mixed with 400 µL deionized water under magnetic stirring for 10 h into a paste which was then rolling-coated on a Cu foil. After drying in vacuum at room temperature, the coated Cu foil was cut into circular pieces (diameter: 14 mm, active material loading: ~0.55 mg cm^{-2}, working electrode) and assembled with a Li metal disc (counter-reference dual-electrode), and a separator of the polypropylene-based Celgard 2400 of the same diameter into a button half-cell in a glove-box. The same electrolyte was used to drop on both sides of the separator directly. Finally, the assembly was converted in a hydraulic sealer into the button half cell or simply button cell in the following text for further electrochemical tests.

Electron microscopic and electrochemical analyses

Field emission scanning electron microscopy (PHILIPS, XL30TMP) was used to study the surface microstructure of the active material filled in the hole of the Cu-MCE before and after recording the CVs. The distribution of elements in the sample was studied by energy dispersion X-ray spectrometry (EDS, OXFORD IET200). Cyclic voltammetry (CV) and electrochemical impedance spectrometry (EIS) of the Cu-MCE and the button half-cells were conducted on the electrochemical workstation (BioLogic, VMP3) at potential scan rates of 0.1 mV s^{-1}, 0.2 mV s^{-1}, 0.5 mV s^{-1}, 1 mV s^{-1}, 2 mV s^{-1} and a frequency range of 10 - 100 MHz, respectively. The potential test range was from 0 to 1.5 V vs. Li/Li^+.

Results and discussion

Structure and characterization of Cu-MCE

Fig. 1a illustrates schematically the Cu-MCE. It was used as the working electrode with the testing material filled in the circular hole (cavity). Fig. 1b shows the electrochemical cell with the Cu-MCE. A Li disc attached to a copper wire by wrapping was used as the counter and reference dual-electrode. 1.0 mol L^{-1} $LiPF_6$ in the mixture of EC and DMC with a volume ratio of 1:1 with 10 % FEC as additive was used as the electrolyte.

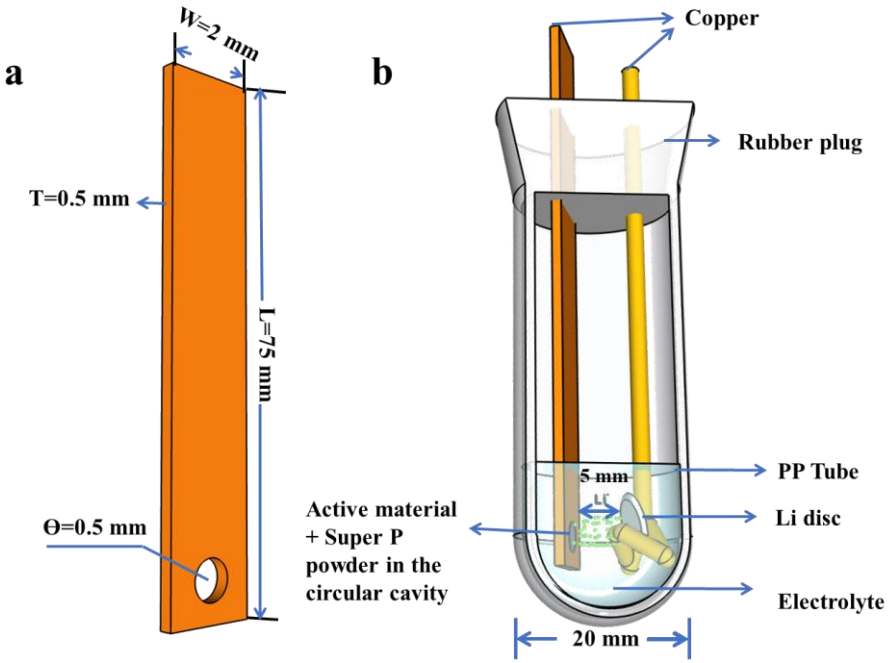

Fig. 1. Schematic illustrations of (a) the Cu-MCE and (b) its arrangement in the electrochemical cell.

It is well known that binders play an important role in affecting the structure, morphology and performance of Si-based electrodes, and have been investigated widely in various half- or full-button-cells. Cu-MCE provides a unique way to observe the behaviour of Si-based negatrodes and the respective changes without the influence of binder. The SEM image of an empty Cu-MCE is presented in Fig. 2a, confirming the cavity to be a circular hole of 500 μm in diameter. Unlike the smooth and flat surface of the Cu foil, both Figs. 2a and 2b show that the inner surface (wall) of the cavity was uneven, resulting likely from drilling caused plastic tearing of the highly ductile Cu. This uneven wall was considered to be beneficial to increasing the specific surface area and enhancing the contact between the active material and the current collector. It was found via dozens of tests and weighing that up to 23.6 ± 1.5 μg of the mixed powders (or 16.5 ± 1.5 μg of Si or P doped Si) could be filled into the circular cavity with two flat sides in contact with the electrolyte.

As confirmed by the SEM image in Fig. 2c, the active material powder filled in the cavity had fairly flat side surfaces, which should help result reproducibility. EDS elemental analysis of the filled Cu-MCE before any test showed that Si and C were both uniformly distributed in the cavity as shown by the EDS measured elemental maps along the right side of Fig. 2c. This indicates that the materials were mixed uniformly during the grinding process. The signals of Si and C were at the noise levels on the Cu foil surfaces outside the cavity.

It is worth mentioning that the volume of the circular cavity was calculated to be 0.098 mm^3. Thus, the packing density of the mixed powders in the cavity should be 0.24 g cm^{-3} which may be translated to a porosity above 85 %, assuming the densities of the 200 nm Si particles and carbon black to be 2.0 and 1.5 g cm^{-3}, respectively. This estimate is very high against the SEM images in Fig. 2c to 2g in which the porosity should be between 40 % to 60 %. However, if the individual particles were microporous, the overall porosity could be much larger than what

appeared in the SEM images. Nevertheless, it can still be concluded that the manually filled powdery mixture packed inside the cavity was highly porous and able to soak in enough liquid electrolyte to ensure high accessibility to reaction sites and easy paths for the movement of ions.

CVs of the empty and filled Cu-MCE were recorded for 5 cycles at a scan rate of 0.2 mV s^{-1}, and the negative limit of the potential scan was set to be 0.01 V vs. Li/Li^+. The SEM images of the filled Cu-MCE are shown in Fig. 2c and 2e before, and 2d and 2f after the five CV cycles. Peeling-off or loss of material was not observed in the cavity, whilst the graininess on the surface of the material in the cavity became smoother, possibly due to the formation of the SEI on the surface of the material. However, a few cracks can be seen in Fig. 2d, but not in Fig. 2c, apparently resulting from repeated volume expansion and contraction during potential cycling. The SEM images in Fig. 2e and 2f show the micro morphologies of materials before and after recording 5 cycles of CVs, respectively. The image in Fig. 2g was recorded on a sample whose potential was scanned to and held at 0.0 V vs. Li/Li^+ for 10 min to ensure full reduction.

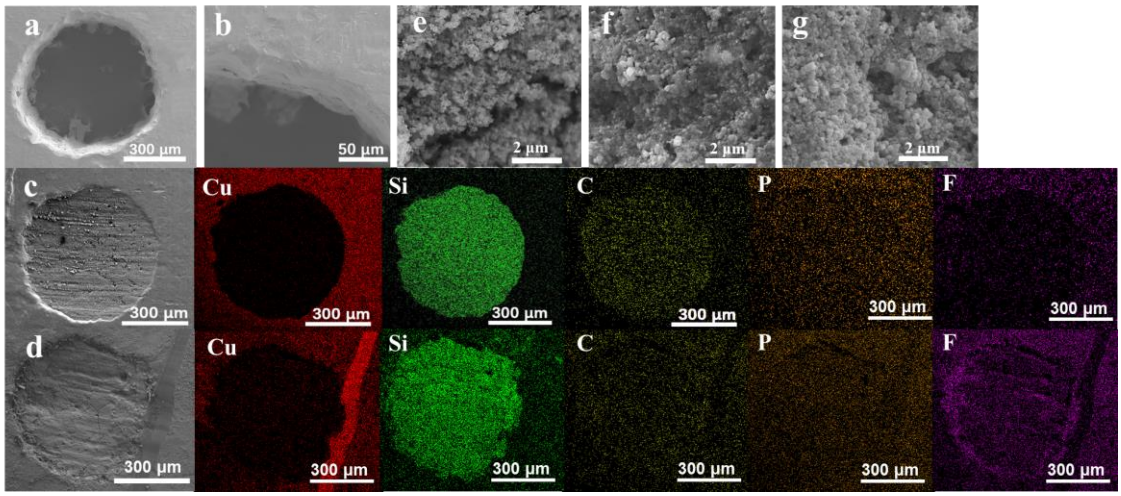

Fig. 2. SEM images of (a) the whole, and (b) part of the rim and wall of the empty circular cavity, (c, e) the cavity filled with the active material before and (d, f) after recording 5 cycles of CVs. The color images along the right side of (c) and (d) are the corresponding EDS mapping of the electrode, and (g) the active material filled in the cavity after scanning the potential to and then held at 0.0 V vs. Li/Li^+ for 10 min.

In addition to the expected porous structure of packed powders, the particles in Fig. 2f and 2g are apparently larger and more agglomerated (or less visible individually as they were partly embedded in, or engulfed by a featureless mass) than those in Fig. 2e. According to the 5th CV, it can be derived that delithiation had proceeded to nearly 90%, which is in accordance with the morphology in Fig. 2g. These changes may be attributed to the volume expansion of, and formation of the SEI layer on and between individual Si particles after repeated de-/lithiation. Another and more possible origin for the featureless mass is the dried lithium salt from the electrolyte, which agrees with the detection of P in the Si filled Cu-MCE after 5 CV cycles as discussed below. It is worth noting that the SEM image in Fig. 2e is not as clear as those in Fig. 2f and 2g, which can be attributed to the lithiated samples being more conducting than the unreduced Si sample.

Results from EDS mapping of Cu, Si, C, P and F in the area of, and around the cavity filled

with the active material before and after 5 potential cycles are shown along the right sides of Fig. 2c and 2d. In the Cu and Si maps, clear borders can be seen interfacing between Cu and the filled powder, confirming the expectation that Cu does not react with either Si or Li. Therefore, copper is a suitable MCE material for studying lithium storage materials and offers high conductivity, low material cost, and easy processing.

For both Si and C, the mapping did not reveal obvious differences inside the cavity before and after the 5 CV cycles. This is indicative of the elemental composition remaining very much unchanged as expected during de-/lithiation which should only add lithium into the material, but lithium is not detectable by EDS. However, the Si and C maps after 5 CV cycles showed detection of the two elements outside the cavity. The finding of Si only in the top-right corner of the Si mapping image outside the cavity could have resulted from an operational incident that scratched some powder particles from the cavity to the Cu foil surface. However, C was detected all over the mapping image. A plausible explanation is the complexes formed between Li^+ and the organic carbonate molecules that were left all over the Cu foil after the electrolyte was dried. Similarly, electrolyte drying should have also left behind the $LiPF_6$ salt, which is evidenced in the P map of the filled Cu-MCE presenting only background noises before any tests, but clear P signals after the 5 CV cycles. In addition, due to the SEI formation and the dried residual electrolyte on the whole surface of the Cu-MCE immersed in the electrolyte, there were obvious F signals outside the cavity, including the scratched region which can also be seen in the other elemental maps after recording the CVs.

In summary, the Cu-MCE is convenient to use for quick microscopic observation and analysis of de-/lithiation caused changes in morphology, microstructure, and composition of the active materials. Analysis of the filled Cu-MCE can avoid testing errors from disassembly of the cell and electrodes and re-assembly of the material samples for analysis, which is inevitable when using the button cell. As will be described and discussed in detail below, the Cu-MCE can also offer fast electrochemical analysis of the active material because the very small volume of active materials minimized the impact of dynamic barriers and complications, such as ion diffusion through the pores between the packed powder particles.

Electrochemical performance of Si and P-doped Si powders in Cu-MCE

The electrochemical performances of Si and P-doped Si powders were investigated by both the Cu-MCE and button cell. Fig. 3a shows the CVs of an unfilled Cu-MCE. A large reduction peak (C1) centered at about 2.3 V vs. Li/Li^+ was observed. This fairly symmetrical peak C1 is indicative of a surface confined process, excluding the reduction of any species in the electrolyte. The rest potential for starting the potent scan was 2.8 V at which anodic oxidation or anodization of Cu must have occurred. It is therefore very likely that peak C1 resulted from the reduction of the anodization product on the copper surface of the Cu-MCE. As expected, the same peak C1 also appeared when the Cu-MCE was loaded with Si or Si-P340 as shown in see Fig. 3b and 3d. Note that the current axis of Fig. 3a differs from those of Fig. 3b and 3d, but peak C1 on these CVs showed comparable currents of the same order of magnitude.

For confirmation of the above attribution of peak C1, CVs were recorded in a less positive potential range from 0 to 1.5 V as shown in the inset of Fig. 3a. It can be seen that at less positive potentials, the CV current varied insignificantly between −0.005 (cathodic) and 0.005 mA (anodic) without any apparent redox peak. These results indicate that the Cu-MCE was

sufficiently stable and could be used as a stable current collector for investigation of Si-based materials without affecting the lithiation reactions between 0 and 1.5 V.

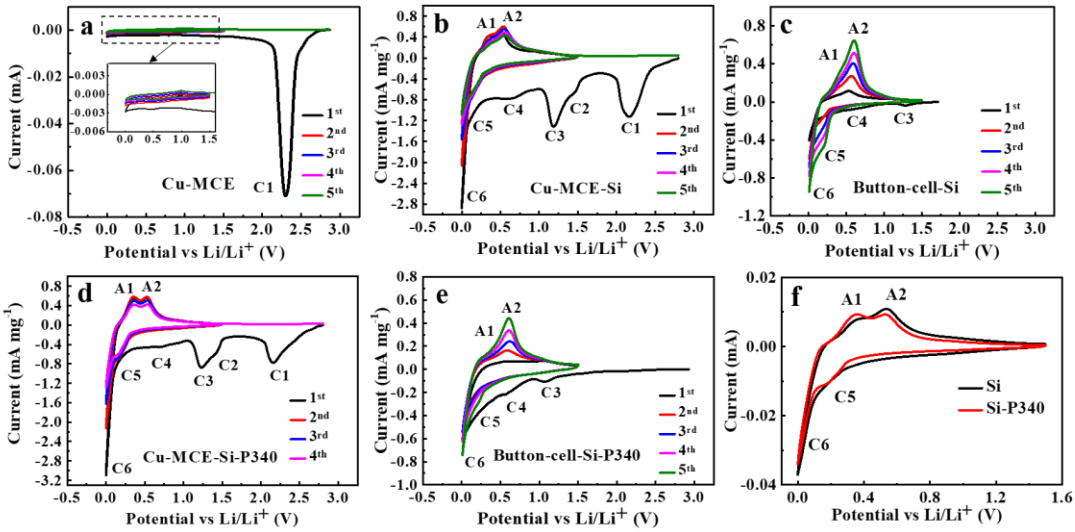

Fig. 3. CVs of the first 5 cycles at the scan rate of 0.2 mV s^{-1} of (a) an empty Cu-MCE, (b) Si in Cu-MCE and (c) in button cell, (d) Si-P340 in Cu-MCE and (e) in button cell. (f) CVs of pure Si and Si-P340 in Cu-MCE. The inset in (a) is the enlarged view of the CVs recorded in the potential range where characteristic responses of silicon are expected.

For comparison, the undoped Si powder was investigated by cyclic voltammetry in the Cu-MCE and button cell respectively at a potential scan rate of 0.2 mV s^{-1}. Typical results can be seen in Fig. 3b and 3c. Here, the specific current is used to discuss the CVs. In some cases with a unmodified planar electrode, current density, i.e. current normalized against area, is used while discussing the electrochemical performance. However, for electrodes loaded with powdery active materials, there are at least three area parameters, namely the apparent surface area of the active material in contact with the electrolyte, the geometric area of the current collector in contact with the active materials, and most importantly the real surface area of the powdery active materials, which is measurable using an appropriate gas adsorption method. Of these, the first two have little theoretical importance and are not suitable for comparison between electrodes of different geometries and structures. The specific surface area of the powdery active material is more commonly used for comparative studies. Because the specific surface area is proportional to the mass (weight) of the powdery active material, the real current density of the electrode is proportional to the mass normalized current. Therefore, we used specific current in this study. In the Cu-MCE filled with SiNPs, the real area could be estimated by the specific surface area of SiNPs, which is about 670 mm^2. With this estimate, the current densities were found to be comparable between the MCE and button half cell and proportional to the specific currents. The characteristic electrochemical reaction peaks of de-/lithiation of Si appeared on the CVs of both the Cu-MCE and button cell. In the first cycle, irreversible reduction peaks, C2, C3, and C4, appeared between 0.5 and 1.7 V. These peaks disappeared on the CVs of the following cycles, indicating an origin from the irreversible formation of SEI during the first cathodic potential scan.

For both the Cu-MCE and button cell loaded with Si, on each CV, two cathodic peaks, C5

and C6 between 0.4 and 0 V, and two anodic peaks, A1 and A2 between 0.2 and 0.6 V were recorded. Because these peaks were absent on the CVs of the empty Cu-MCE, they can be attributed to the lithiation (C5, C6) and delithiation (A1, A2) reactions of Si. These preliminary observations are in agreement with the basic characteristics of the electrochemical reaction of Si-based materials, confirming the suitability of using both devices in this work.

However, there are differences between the CVs of Si-based materials in the Cu-MCE and button cell. Firstly, the currents on the CVs of the button cell are much smaller than those of the Cu-MCE. For example, the peak current of A2 was actually 0.55 mA on the 5^{th} cycle CV of the button cell in Fig. 3c, but only about 0.08 mA in the CVs of the Cu-MCE in Fig. 3b. This difference is basically because of the different amount of Si loaded in the button cell (0.85 mg) and the Cu-MCE (0.0165 mg). Nevertheless, the mass normalized anodic current of the Cu-MCE agreed fairly well with that of the button cell, considering experimental errors, particularly when weighing the Cu-MCE. The much smaller currents of the Cu-MCE are beneficial for electroanalytical purposes as discussed below.

Secondly, the smaller amount of Si in, and hence the lower current of the Cu-MCE should help reduce polarizations and reveal more details of Si de-/lithiation on the electrode. It is worth mentioning that in any electrochemical cell or electrode, polarization is directly proportional or stongly related to the absolute current flowing through the cell or electrode. For more details, for example, the Cu-MCE CVs in both Fig. 3b and 3d show very well-resolved peak A1 from peak A2, but these two anodic peaks are basically merged in the CVs of the button cell in Fig. 3c and 3e. Upon cathodic polarization, it can be seen that both peaks A1 and A2 occurred on the first cycle CV of the Cu-MCE and remained almost unchanged on the CVs of the following cycles. This is evidence of the benefits from the small and circular geometry of the MCE to the charge transfer reaction which starts at the cavity wall where the "Cu | Si | electrolyte" (for reduction) or "Cu | Li_xSi | electrolyte" (for oxidation) three-phase interlines (3PIs) are converted to the "Li_xSi | Si | electrolyte" 3PIs in the beginning. Because the electrolyte can access the active material from both sides of the MCE, the longest distance for ions to transport inside the active material is 250 μm. The newly formed Li_xSi | Si | electrolyte 3PIs then propagate into the center of the active material filled cavity. In these processes, ion supply or removal was basically three-dimensional in nature and therefore fast. On the contrary, peaks A1 and A2 on the CVs of the button cell in Fig. 2c and 2e grew gradually with cycling, indicating a slowly progressed or activated process. The slower response of the button cell is understandable because, at least partly, the transport of electrons or ions is basically one-dimensional from opposite sides of the coating of active material.

Last, but not least, Si-based materials are semiconductors and hence present a certain level of resistance to a current flow. Additional resistance comes inevitably from the electrolyte, and also the use of the insulating binder and other additives in the electrode. Consequently, ohmic polarizations can result from these resistive factors in proportion to the overall current. In comparison with the Cu-MCE, the button cell was loaded with the binder and much more active material, and output much greater currents, leading to non-negligible ohmic polarization, which is reflected by the shifting peak potential of A2 in Fig. 3c and 3e when the peak current increased significantly. Further observations of ohmic polarization in the button cells are given in Fig. 4, showing CVs recorded at different potential scan rates. In the Cu-MCE, the transportation of both the electron and ion is achieved not only by the planar diffusion from

both sides of the MCE which is in contrast to the semi-planar diffusion in the button half cell, but can also realize in the vertical direction, leading to much faster dynamics and deeper penetration.

According to repeated experiments under the same conditions, a few more details are worth mentioning. The first oxidation peak A1 at 0.35 V and the reduction peak C6 at about 0.2 V are sharper or more obvious on the Cu-MCE CVs than those of the button cell. These results indicate that the μA-current driven reaction can be studied more accurately and sensitively through the Cu-MCE. In addition, the CV shapes indicate that the electrochemical reactions in the Cu-MCE were more reversible. This may be attributed to less material used, and better contact with the current collector and electrolyte in Cu-MCE. The avoidance of binder in the Cu-MCE and also the much smaller currents could have mitigated the respective influences, thus more accurate results could be obtained about the electrochemical properties of the active materials. In addition, the convenience of avoiding binder with the MCE is unmatchable with the button half cell. At higher scan rates, 7-8 cycles of CV have been applied, revealing similarly good repeatability. However, aiming to quickly revealling the electrochemical performance of electrodes with higher accuracy, better details, and greater efficiency, the Cu-MCE is not designed with very long durability.

Fig. 3d and Fig. 3e compare the CVs of Si-P340 in the Cu-MCE and button cell respectively. The CVs are similar to those of undoped Si, demonstrating that the characterization with Cu-MCE filled with active material is quite universal and reproducible. The oxidation peaks A1 and A2 of Si-P340 near 0.35 V and 0.54 V, and the reduction peak C6 around 0.2 V are more pronounced than those of the commercial Si powder (Fig. 3b and Fig. 3d). This is understandable because P atoms can enter the Si lattice (i.e. P doping), forming an n-type semiconductor.[21] According to ICP-AES measurements, the concentration of P atoms was around 3×10^{18} cm^{-3}, corresponding to an atomic P/Si ration of about 10^{-4}, which is below the limit of dissolution of P in solid Si, which means all doped P would be electro-active for ionization, $P \rightleftharpoons P^{+} + e^{-}$. Consequently, the electronic conductivity of the Si-P340 powder should be higher than the commercial Si powder, which is beneficial to de-/lithiation. Similar conclusions can be obtained from the CVs of the button cell.

Moreover, the characteristic reaction peaks of Si-P340 in the Cu-MCE were sharper, and the reaction potential could then be characterized more accurately. Since the Cu-MCE was filled with a much smaller amount of active materials, at the same voltammetric time scale, the electrode reaction could proceed to completion in a shorter time, which can translate into greater analytical sensitivity. For example, a slight current change caused by material phase change could be detected more accurately on the CVs. In this work, on all CVs, the cathodic peaks between 0.45 V and 0.01 V were the superposition of reactions in different stages of the formation of different Si-Li compounds. The anodic peaks between 0.2 V and 0.6 V also corresponded to the superposition of a series of reactions of Li separation from the Si-Li compounds. According to the literature, Si-based materials undergo the following transformations during the lithiation and delithiation processes. The crystalline Si goes through a crystalline-to-amorphous phase transformation during the first lithiation to form a series of amorphous Li_xSi alloys (actually the stoichiometric compounds depending on the applied potential changes). The $Li_{15}Si_4$ phase would form when the potential of electrode is around 60 (50) mV. [22-24]

Lithiation process:

$$Si + Li^+ + e \rightleftharpoons LiSi \quad (1)$$

$$3LiSi + 4Li^+ + 4e \rightleftharpoons Li_7Si_3 \quad (2)$$

$$4Li_7Si_3 + 17Li^+ + 17e \rightleftharpoons 3Li_{15}Si_4 \quad (3)$$

Delithiation process:

$$3Li_{15}Si_4 \rightleftharpoons 4Li_7Si_3 + 17\,Li^+ + 17e \quad (4)$$

$$Li_7Si_3 \rightleftharpoons 3LiSi + 4Li^+ + 4e \quad (5)$$

$$LiSi \rightleftharpoons Si + Li^+ + e \quad (6)$$

In the above reactions, the two lithiation reactions (1) and (2) occur at very close potentials to form Li_7Si_3 and are superimposed in the potential range between 0.40 and 0.04 V, corresponding to the reduction peak C5 on the CV. Li_xSi compounds with higher Li contents (maximum at $Li_{4.4}Si$) could form via, and following reaction (3) at potentials up to 0.01 V, leading to peak C6 in the CV. Reduction of Li^+ beyond 0.01 V tends to deposit Li dendrites which may partly limit the delithiation reaction and lead to the capacity loss of Si. Similarly, the transformation from Li_xSi compounds to amorphous Si occurs during delithiation. Firstly, high Li content compounds, e.g. $Li_{3.16}Si$, are delithiated to form Li_7Si_3 (4), Li_7Si_3 to form LiSi (5), and finally, LiSi to Si (6).[22] In Fig. 3b and Fig. 3c, the oxidation peak A1 at 0.35 V corresponds to the delithiation reaction (4), which is attributed to the phase transition from $Li_{3.16}Si$ to Li_7Si_3. The oxidation peak A2 at 0.54 V corresponds to reactions (5) and (6).

In Fig. 3f, the second cycle CVs of Si and Si-P340 in Cu-MCE are compared to further verify the usefulness of this electrode. P-doped Si is known to have higher conductivity and greater tolerance to volume changes than pure Si but not alter the mechanisms of de-/lithiation of Si. Therefore, the differences between P-doped Si and Si on CVs can be kinetic and/or dynamic in nature. Such differences can be subtle on CVs, but should lead to better resolution of current peaks and reversibility of the shapes, e.g. smaller separation between the paired cathodic and anodic peaks, and smaller or no shift in peak potential against potential scan rate variation.

The scan rate used for recording the CVs in Fig. 3f was 0.2 mV s^{-1}, which was thought to be sufficiently slow so that influences from ohmic and kinetic polarization can be sufficiently small or insignificant. As expected, Fig. 3f shows that both materials underwent two reduction and two oxidation steps. The two reduction steps that converted Si to Li_xSi compounds started around 0.20 V (C5) and then proceeded into a fast-increasing current in the potential range between 0.04 and 0.10 V (C6). The two oxidation steps which were caused by delithiation of the Li_xSi compounds appeared as current peaks at about 0.35 (A1) and 0.54 V (A2). These similar CVs suggest that both doped and undoped silicon materials underwent the same electrode reactions. Nevertheless, for the P-doped sample, several changes are visible on the CVs. Firstly, peaks C5 and A1 both became more pronounced, i.e. better resolved, particularly

the relative height of A1 increased. Secondly, the potential difference between the cathodic and anodic peaks narrowed, indicating either or both of lower ohmic polarization and better kinetic and dynamic performances, which translates to greater reversibility of the electrode reactions. The area enclosed by the CVs of P-doped material was also larger, indicating an increase in the reversible lithium storage capacity. This improvement should more likely result from electrons being able to access more reaction sites, instead of P-doped Si having a greater lithiation capacity than Si. In other words, the higher conductivity and greater volume change tolerance of P-doped Si should be responsible for the enhanced de-/lithiation. According to the literature, P doping not only generates more vacancy in Si as the dominant factor contributing to the increased conductivity,[25, 26] but also enables lattice distortion to a greater degree and hence larger tolerance for volume expansion.[27]

The electrode reaction process involves two main steps, namely (1) the transfer of electronic and/or ionic charge at an appropriate phase boundary, e.g. the Si/Cu or Si/electrolyte interface, and (2) the transport of ions or molecules towards or away from the reaction boundary. In other words, kinetics studies charge transfer reactions whilst dynamics studies mass transport. In some cases, dynamics are considered to be part of kinetics. Specifically, these two main processes occurr during the lithiation/delithiation of silicon, whilst the reaction kinetics is decided by the alloying process of silicon, and the dynamics is influenced by the mass transport during charging/discharging. To analyze the electrochemical reaction kinetics and charge transport mechanism or dynamics in the active materials during de-/lithiation, CVs at different scan rates were recorded. Fig. 4a and Fig. 4d are the CVs of the Cu-MCE and the button cell of the undoped Si powder after activation at scan rates of 0.1, 0.2, 0.5, 1.0, and 2.0 mV s^{-1}. The potentials of the anodic and cathodic peaks on the Cu-MCE CVs remained unchanged when increasing the scan rate, while both the anodic and cathodic peak currents increased with increasing the scan rate. These features indicate the high reversibility of the electrode reactions. It can also be noted that peaks A1 and A2 were clearly separated on the Cu-MCE CVs until the scan rate reached 2 mV s^{-1}. At 2 mV s^{-1}, the Cu-MCE CV showed a broad anodic peak which seemed to have resulted from peak A1 becoming more dominant. However, on each CV of the button cell, peak A2 remained dominant with peak A1 being almost engulfed. It became broader and shifted to more positive potentials at higher scan rates. These CV features indicate (1) higher ohmic and concentration or dynamic polarizations in the button cell, (2) faster electrode kinetics and dynamics in the Cu-MCE, and (3) variation in the kinetics of different oxidation stages with increasing the scan rate. Particularly, the CVs of the Cu-MCE indicate that A2 was slower than A1 in response to the increasing scan rate, but this change was not recorded on the CVs of the button cell.

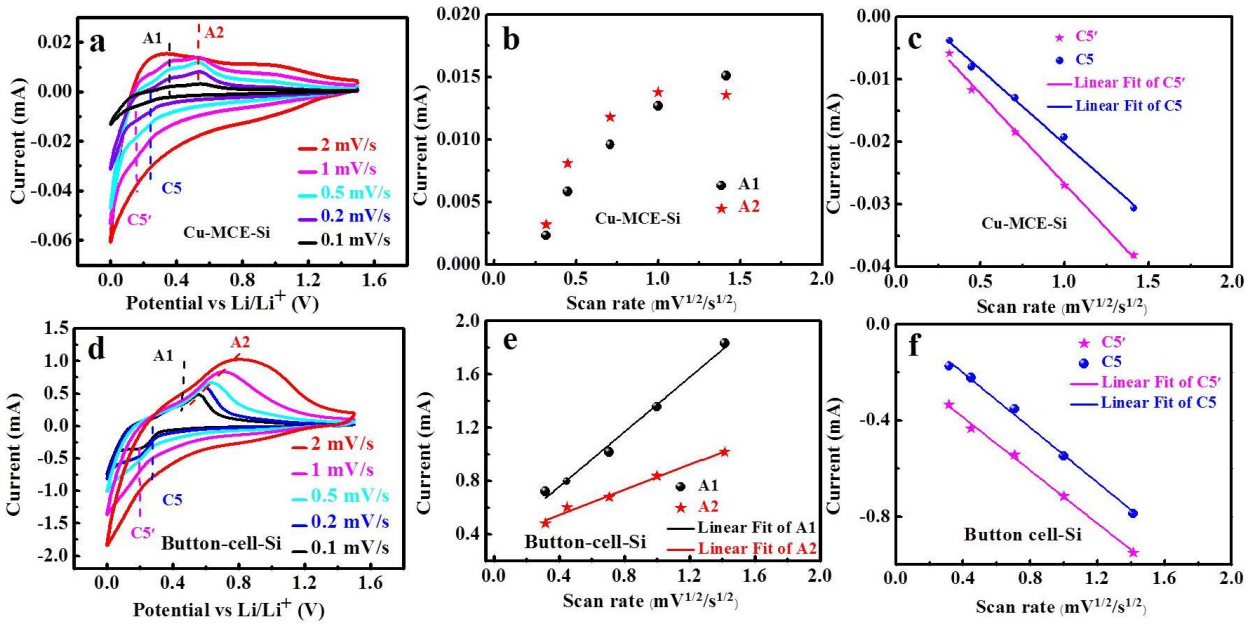

Fig. 4. CVs of Si at scan rates from 0.1 to 2 mV s^{-1} in (a) Cu-MCE and (d) button cell. Peak currents at various scan rates of Si in Cu-MCE (b, c) and button cell (e, f).

Dynamic and kinetic analyses

Further comparison was made between the Cu-MCE and the button cell for electrochemical de-/lithiation of Si-based materials against reaction kinetics and electrode dynamics, by fitting the CVs data with the following equation [28-31]:

$$i = k_1 v + k_2 v^b \quad (7)$$

where i is current, v the scan rate, b the surface-diffusion control parameter, and k_1 and k_2 are coefficients. When b = 1, the equation could be simplified as $i = (k_1+k_2)v$. Thus, the current is proportional to the scan rate, which shows that the rate of the electrode process depends only or dominantly on an electrode surface or electrode confined process involving charge transfer or storage. In other words, the surface-confined reaction is the slowest step, and hence controls the overall rate of the electrode process. Such an electrode process is often termed as a surface-confined process in electrochemical literature, although the same principle applies more widely in many other electrodes confined processes, such as the thin layer electrode and the cavity electrode [18,19]. In this article, the term of surface confined process is still used for consistency with the literature, although the more accurate term is electrode confined process.

When b = 0.5 and $k_1 = 0$ (or $k_1 << k_2$), the equation becomes $i = k_2 v^{1/2}$. The current is proportional to the square root of the scan rate, indicating that diffusion which is a dynamic phenomenon, is the slowest step, and hence controls the overall rate of the electrode process. Such a process is known as a diffusion-controlled process.[33] In some literatures, the surface-confined process was defined as the capacitive mode, while the diffusion-controlled process was defined as the battery mode. The ratio of the contributions of battery to capacitive was calculated according to this analysis. However, in typical battery-like material, there still exists

surface reaction processes that are not controlled by diffusion, and there are similar facts in capacitive material. Therefore, we only discuss the diffusion-controlled process and the surface-confined process in this section.

It is worth mentioning that charge and/or mass transport (not transfer), particularly diffusion, is a dynamic phenomenon, but it is often attributed to causing kinetic complications. This is because diffusion occurs before (and after) electron transfer reactions (or charge storage processes) on electrode and can alter the kinetics or relative rates of parallel but different steps of electrode reactions. Consequently, many authors do not consider the dynamic nature of diffusion when reporting and discussing electrode processes, but simply attribute diffusion to being part of electrode kinetics. In this work, a main benefit from using the Cu-MCE is the reduced influence of diffusion dynamics, instead of changing the mechanisms and kinetics of the electrode reaction. Specifically, equation (7) is known for electrode kinetics, but only the first term is for kinetics, but the second term is for dynamics.

The oxidation peak currents at 0.35 V (A1) and 0.54 V (A2) extracted from the CVs of the Cu-MCE and the button cell are plotted *vs.* $v^{1/2}$ in Fig. 4b and Fig. 4e, respectively. For the CVs of the Cu-MCE, the plots for the two oxidation peaks were nonlinear, indicating that delithiation was controlled by both diffusion and surface processes. In the button cell, there was an obvious linear relationship for each of the two oxidation peaks, indicating that delithiation in the button cell was mainly controlled by the semi-diffusion process of Li^+ ions. It should be emphasized that diffusion control leads to concentration or dynamic polarization, and hence is unwanted for any battery design and manufacture. In other words, diffusion control is not an intrinsic or theoretical feature of a properly designed and operated battery electrode, although it is difficult to avoid in practice of high power operation.

For lithiation, CVs in both Fig. 4a (Cu-MCE) and 4d (button cell) do not show an obvious peak, but they are featured by a reduction wave (C5) which should correspond to reactions (4) and (5). Currents were extracted from the two inflexion points of the wave at potentials of 0.16 V (C5') and 0.24 V (C5), and plotted against $v^{1/2}$ in Fig. 4c and 4f. Linear plots were obtained at both potentials, indicating diffusion-control in both the Cu-MCE and button cell during lithiation.

It was reported that during lithiation, the phase transformation from Si to Li_xSi, may enhance Li^+ ion diffusion in Si, and the Li_xSi compound with high x has stronger lithium ion diffusion ability than those with low x.[32, 33] As discussed above, the Li^+ ions are supplied three-dimensionally via the liquid electrolyte in the pores of the Cu-MCE. Following liquid diffusion, Li^+ ions react with solid Si at a sufficiently negative potential to form a surface phase of Li_xSi which allows Li^+ ions to transport through to access fresh Si underneath the Li_xSi phase. Li^+ ions can also transfer between different Li_xSi phases to complete the complicated solid state lithiation process. It is known that solid-state diffusion is usually 6 to 8 orders of magnitude slower than liquid-state diffusion, but the negative influence of solid-state diffusion could have been significantly compromised or mitigated by using ca. 200 nm Si particles in this work. Thus, the linear plots of i vs. $v^{1/2}$ in Fig. 4 could have resulted more likely from Li^+ ion diffusion in the liquid electrolyte in the pores of the Si powder packed in the Cu-MCE or on the surface of the Cu foil of the button cell.

The non-linear i vs. $v^{1/2}$ plots of peaks A1 and A2 in Fig. 4b for the Cu-MCE are interesting and indicate mixed control of diffusion and surface change on delithiation. Because the plots

for lithiation in Fig. 4c are linear, the delithiation of Li_xSi compounds might likely be kinetically and dynamically slower than the lithiation of Si. This may be explained as follows. Lithiation converts the poor conductor Si to the more conducting Li_xSi phases, promoting the overall reaction rate. Delithiation does the opposite, impeding the process. This explanation agrees with the fact that in Fig. 4d for the button cell which output sufficiently large currents, the anodic peak A2 shifted positively with increasing scan rate, but the cathodic wave C5 did not show the same. Further, since delithiation in the button cell was still diffusion controlled as evidenced in Fig. 4e, it can be concluded that the Cu-MCE was indeed beneficial to enhancing liquid state diffusion, which in turn led to an equivalent effect of decreasing the relative kinetic rate of the electrode (or surface) confined solid phase conversion, leading to a mixed control of the overall reaction rate.

The above analysis of the i vs. $v^{1/2}$ relationship at feature current potentials indicates that diffusion was a dominant factor affecting the overall rate of Si de-/lithiation, but surface-confined processes, such as solid phase conversions, also contributed to limiting the overall reaction rate. According to some reports,[34-37] equation (7) was converted to the linear form as given in equation (8) with b = 0.5 to enable the graphical determination of values of k_1 and k_2. Then, the product of either k_1v or $k_2v^{1/2}$ was calculated for each potential of the whole CV and plotted against the potential to show the contribution of either the surface-confined or diffusion-controlled process.

$$i/\sqrt{v} = k_1\sqrt{v} + k_2 \quad (8)$$

Following this procedure, equation (8) was used to derive values of k_1 and k_1v from CVs in Fig. 4a and 4c. The results for CVs recorded at 0.1 and 2.0 mV s^{-1} are presented in Fig. 5a and 5b for the Cu-MCE, and Fig. 5d and 5e for the button cell, respectively. It can be seen that the derived k_1v values are a little unusual for the Cu-MCE, particularly those for the CV at 2 mV s^{-1}, but not too far away from expectation. However, for the button cell, something must have gone wrong because some values of k_1v in the potential range between 0.3 and 0.8 V were negative for the anodic process.

In search for the error in the derivation and calculation, it became apparent that the use of currents on CVs of different scan rates at the same potential to derive the k_1 value was problematic. For example, the CVs in Fig. 4d show that the peak potential of A2 shifted positively, indicating obvious polarization in the button cells. This observation suggests that at the same potential, the currents on CVs of different scan rates do not represent the same electrode process. In such a case, equations (7) and (8) are only applicable at feature potentials such as those for current peaks or inflexions, as shown in Fig. 4b, 4c and 4e and 4f. However, if the polarization is large, plotting current at the same potential against the scan rate may not lead to a linear result as predicted by equation (8). This is evidenced in Fig. 5c and 5f, showing a clear deviation of the anodic current data from linearity. Note that the data points at 0.54 and 0.68 V in Fig. 5c for the Cu-MCE, and those at 0.3, 0.54, and 0.68 V in Fig. 5f for the button cell show a trend that will give negative slopes, and hence negative k_1 values if a linear fitting is forced through the relevant data points.

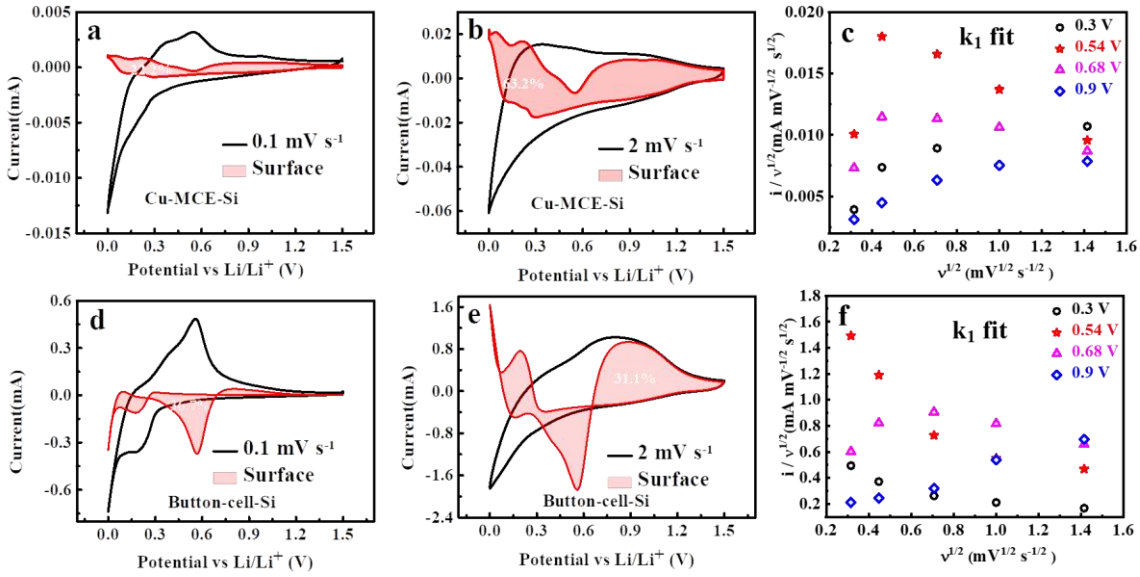

Fig. 5. CVs (black lines) and calculated currents (red line shaded areas) from electrode confined process at 0.1 mV s^{-1} and 2.0 mV s^{-1} of the Cu-MCE (a, b) and button cell (d, e). The scatter plots of $i/\sqrt{v}$ vs. $1/\sqrt{v}$ in the Cu-MCE (c) and the button cell (f) for the anodic currents.

Electrode polarizations can result from either slow reaction kinetics, mass transport dynamics and non-negligible electrode and electrolyte resistance. These three types of polarization become more influential with increasing the electrode current by for example using more active materials on the electrode and higher potential scan rates. This polarization-current correlation also explains why the problem was more serious in the CVs of the button cell (more active materials and hence larger currents) than those of the Cu-CME, and also on CVs at higher scan rates (2.0 mV s^{-1}) than those at lower scan rates (0.1 mV s^{-1}).

It is worth pointing out that the CVs of both the Cu-MCE and button cells indicate that the de-/lithiation of Si-based materials involve multi-electron transfer in multiple steps, in agreement with the literature.[25,26] Therefore, in addition to ohmic polarization, kinetic and/or dynamic polarizations may result from not only the slow rate of the control step but also the different responses of different steps to the variation of potential scan rate. The latter is supported by the fact that peaks A1 and A2 on the CVs of the button cell responded very differently to increasing the scan rate as shown in Fig. 4c. Such kinetic and dynamic complications were absent or much less obvious on the CVs in Fig. 4a, indicating an advantage of using the Cu-MCE for more reliable electrochemical analyses. Therefore, Li^+ ion diffusion is important to understand and improve the performance of Si-based negatrodes.

To further investigate the kinetics and dynamics of silicon-based negatrode materials in both the Cu-MCE and button half cell, electrochemical impedance spectroscopy (EIS) was performed in both cells at paired potentials of 1.5 and 1.0, 1.5 and 0.4, and 1.5 and 0.1 V, and 1.5 V successively. At each potential, the cell was kept for 5 minutes before the EIS test. To eliminate the influence of oxide reduction or anodization on the Cu surface, a prior CV cycle was applied to the Cu-MCE between 0 and 1.5 V at 0.2 mV s^{-1}.

Fig. 6a-b shows the specific EIS (mass normalization) of silicon material in the Cu-MCE

and button half cell, and the inset in Fig. 6b shows the enlarged view of the high frequency region. All EIS plots are composed of one or two semicircles in the high and middle frequency region. Whilst a tilted straight line appeared at low frequencies in most cases, more complicated behavior was observed at potentials close to that for Li deposition as shown in Fig. 4c-f. The semi-circle in the high frequency region is corresponding possibly to the charge transfer resistance or the Faradaic reaction kinetics.

The tilted straight line in the low frequency region reflects the mass transfer dynamics, and the specific diffusion resistance in the button cell is nearly ten times larger than that in Cu-MCE, indicating improved ion transport dynamics in the MCE. It is worth noting that the four spectra at 1.5 V of Cu-MCE exhibit similar impedance distributions, indicating the stable expression of the reaction kinetics and dynamics in Cu-MCE. However, the specific diffusion resistance in the button half cell at the low frequency varied in the four spectra at 1.5 V. It was noted that the spectrum at the first 1.5 V showed relatively low overall impedance, suggesting the influence of Cu foil since the EIS plots were recorded on the as-received cell without the prior CV cycle treatment as in the case of the Cu-MCE.

The next three EIS plots at 1.5 V exhibited a gradual decrease diffusion resistance but similar reaction kinetics, implying the slow activation process which was also observed on the CVs in Fig. 3c and 3e. Fig. 6c-d shows the EIS of Si material at 1.0 V in both Cu-MCE and button half cell. There is a flattened or broad semi-circle in the spectrum of the Cu-MCE, but a small and a large semicircles appeared in that of the button half cell. It can be noted that the radius of the semicircle in the Cu-MCE spectrum is approximate to that of the small semicircle in the spectrum of the button cell. Considering its higher frequency range, the small semicircle should be more likely related to the electron transfer resistance while the larger semicircle at middle frequencies to the ion transfer resistance.

An equivalent circuit is shown in the inset of Fig. 6c, where R_{el} is the electrolyte resistance, R_{et} is the electron transfer resistance, and R_{it} is the ion transfer resistance. It can be seen that R_{el} and R_{it} measured in the Cu-MCE are similar, about 53 Ω, while R_{el} and R_{it} in the button cell are 52 Ω and 716 Ω, indicating a much larger ion transfer resistance in the button cell than that in the Cu-MCE. Fig. 6e and 6f show the EIS of Si in both Cu-MCE and button half cell at the potential of 0.4 V and 0.1 V, respectively. Interestingly, the spectra at 0.4 V in both cells exhibit distinct shape at low frequencies. It is supposed that at 0.4 V the lithiation reaction begins, which may need a longer time to reach the equilibrium state and therefore the resistance may be still varying during the EIS measurement.

In Fig. 6e and 6f, the EIS plots recorded at 0.1 V shows clearly smaller resistance to both electron and ion transfer. Particularly the middle frequency semicircle on the spectra of the button half cell decreased much more significantly than the high frequency one. This is an interesting phenomenon considering that in the button half cell, an activation process is needed before the Si-based active material becomes fully functional. This observation is thus indicative of that the activation could be more relevant to ion transfer than electron transfer. Indeed, no sign of activation was observed on the CVs of the Cu-MCE in which ion transfer and transport are both promoted. The low frequency impedance behavior of both the MCE and button cell at 0.1 V was complex, suggesting additional charge transfer reactions mixed with dynamic control. Further work is needed for a better understanding.

To further verify the ion diffusion dynamics, the Li^+ ion diffusion coefficient, D_{Li^+}, was

calculated according to the following equation:[38, 39]

$$D_{Li^+} = \frac{R^2T^2}{2A^2n^4F^4C^2\sigma^2} \quad (9)$$

Where A is the apparent surface area of the electrode, i.e. the contacting area between the active materials and the liquid electrolyte, n is the number of electron transfers in the reaction, F the Faraday constant, C the Li^+ ion concentration, R the gas constant, and T the operating temperature. The Warburg coefficient σ can be calculated by linear fitting according to

$$Z' = R_{el} + R_{et} + R_{it} + \sigma\omega^{-\frac{1}{2}} \quad (10)$$

where Z' is the real part of the impedance, and ω the angular frequency. The values of D_{Li^+} were found to be 2.24×10^{-10} cm^2 s^{-1} and 7.4×10^{-16} cm^2 s^{-1} in Cu-MCE and button half cell, respectively, suggesting different ion transportation processes in the two cells.

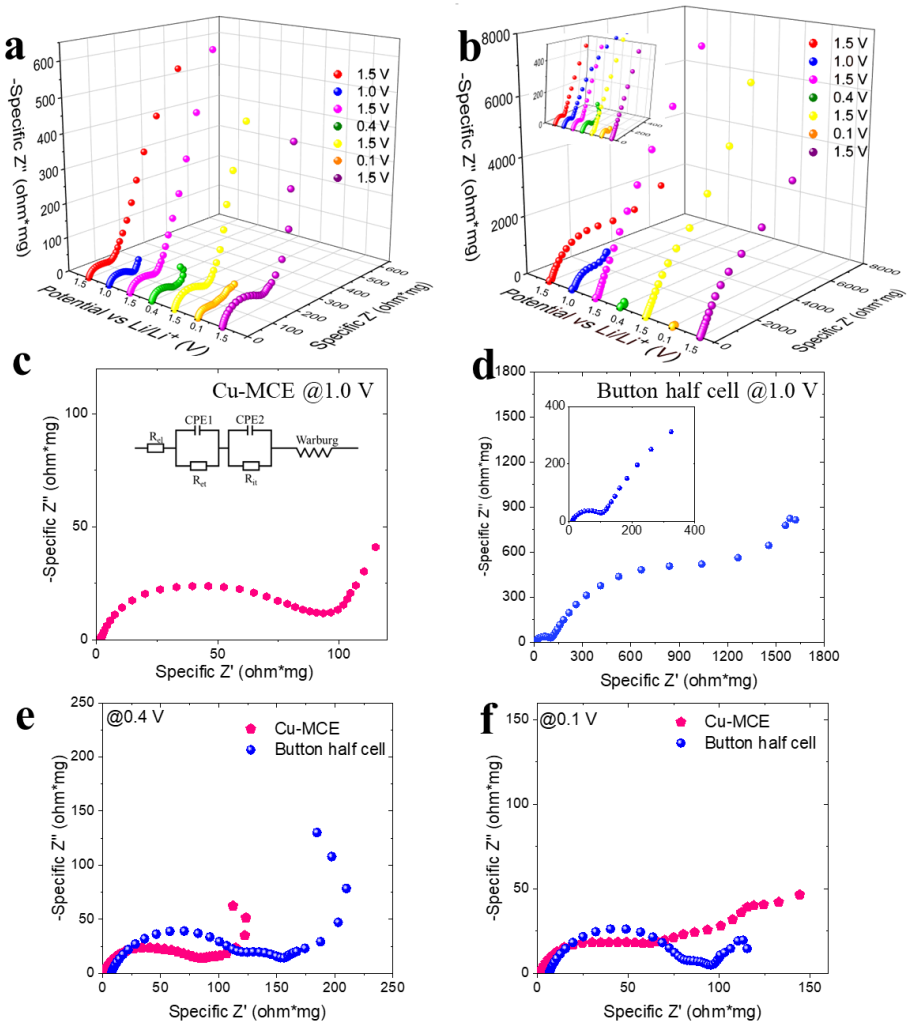

Fig. 6. EIS of silicon material in (a) Cu-MCE and (b) button half cell at different potentials. The cells were controlled for 5 minutes at potentials of 1.5 V, 1.0 V, 1.5 V, 0.4 V, 1.5 V, 0.1 V, successively, and back to 1.5 V. The EIS of silicon material at 1.0 V in (c) Cu-MCE (the inset is the equivalent circuit) and (d) button half cell (the inset is the enlarged image at high frequency region.) The EIS of silicon material in Cu-MCE and button half cell at potentials of (e) 0.4 V and (f) 0.1 V.

Conclusions

With a novel copper foil based metallic cavity electrode (Cu-MCE), silicon (Si) and phosphorous-doped silicon (P-doped Si) materials have been studied by cyclic voltammetry and electrochemical impedance spectroscopy for lithiation and delithiation. Whilst similar main features were observed in these two measurements, obvious differences can be attributed to the very different electrode structures and the presence and absence of the binder, and then to the MCE being capable of promoting ion transport dynamics.

The initial apparent electron transfer reaction area of the MCE (0.785 mm^2) is much smaller than that of the half-button cell (153.86 mm^2), leading to a significantly lower polarization in the MCE. In comparison with the conventional button cell, the Cu-MCE uses much smaller amounts and volumes of the active material (10 to 20 micrograms) without addition of any binder material, and can thus facilitates reactive and non-reactive processes in terms of electron transfer kinetics and ion transport dynamics. It was confirmed in this work that the Cu-MCE provided more accurate, detailed, and direct reaction information in a shorter time. More specifically, the number of reaction steps and their main features on the cyclic voltammograms (CVs) of a commercial silicon powder recorded using the Cu-MCE were in accordance with, but more pronounced and detailed than their counterparts from the button cell. In addition, the slight differences in reaction mechanism between Si and P-doped Si samples were revealed on the CVs recorded using the Cu-MCE. The oxidation peak currents at 0.35 V and 0.54 V, and the reduction peak currents at 0.165 and 0.245 V on the CVs of the Cu-MCE were plotted *vs.* $v^{1/2}$, respectively. The CVs showed two oxidation peaks whose current varied in non-linear manner against the square root of the scan rate, suggesting mixed control of lithiation by both diffusion and surface processes. Similar plots for the two reduction peaks were linear with comparable slopes, indicating similar diffusion-controlled processes. On the contrary, the CVs of the button half cell indicated diffusion control in both lithiation and delithiation, evidencing dynamic difficulties. Further, the Cu-MCE also made it very convenient to carry out microscopic analysis of the microstructure, morphology and elemental composition of the active materials before and after electrochemical tests without breaking up the button cell and disturbing the packing structure of electrode. The EIS results have confirmed the main conclusions from the CVs. Specifically, the EIS measurement revealed noticeable transfer barriers to both electrons and ions, but the ion transfer resistance was much larger in the button half cell than in the Cu-MCE. Similarly, the EIS results also indicated that the specific ion diffusion resistance in the Cu-MCE was much smaller than that in the button half cell.

In addition and more importantly, the Cu-MCE can be inspected directly after dis-/charging without any disturbance to the electrode materials, and provides unseen variation in the packing structure, particle morphology, and elemental information of the active materials. This work has demonstrated that the Cu-MCE is a promising laboratory tool for rapid, effective, reliable, and accurate investigation of the electrochemical and microscopic characteristics of the lithiation and delithiation of Si-based negatrode materials. By filling different existing and new active materials of lithium-ion batteries in the Cu-MCE, detail-exploring and comparative analyses can become convenient and efficient, saving time, effort, and resources in developing new electrode materials.

Acknowledgments

This work was supported by the National Natural Science Foundation of China (No. 51602234) and the Natural Science Foundation of Hubei Province (2021CFB434).

References

[1] Zhao J, Zhao S, Xiawu, Cheng H, and Nan C, Double role of silicon in improving the rate performance of $LiFePO_4$ cathode materials. *Journal of Alloys and Compounds*. 2017. **699**, 849-855

[2] Nitta N, Wu F, Lee J T, and Yushin G, Li-ion battery materials: present and future. *MATTOD Materials Today*. 2015. **18**, 252-264

[3] Ashuri M, He Q, and Shaw L L, Silicon as a potential anode material for Li-ion batteries: where size, geometry and structure matter. *Nanoscale*. 2016. **8**, 74-103

[4] Andre D, Hain H, Lamp P, Maglia F, and Stiaszny B, Future high-energy density anode materials from an automotive application perspective. *Journal of Materials Chemistry*. 2017. **5**, 17174-17198

[5] Liu W, Song M S, Kong B, and Cui Y, Flexible and Stretchable Energy Storage: Recent Advances and Future Perspectives. *Adv Mater*. 2017. **29**, 1603436

[6] Luo W, Chen X, Xia Y, Chen M, Wang L, Wang Q, Li W, and Yang J, Surface and Interface Engineering of Silicon-Based Anode Materials for Lithium-Ion Batteries. *Advanced Energy Materials*. 2017. **7**, 1-28

[7] Wang K, Pei S, He Z, Huang L, Zhu S, Guo J, Shao H, and Wang J, Synthesis of a novel porous silicon microsphere@carbon core-shell composite via in situ MOF coating for lithium ion battery anodes. *Chemical Engineering Journal*. 2019. **356**, 272-281

[8] Ikonen T, Nissinen T, Pohjalainen E, Sorsa O, Kallio T, and Lehto V P, Electrochemically anodized porous silicon: Towards simple and affordable anode material for Li-ion batteries. *Sci Rep*. 2017. **7**, 1-8

[9] Kim S-J, Kim M-C, Han S-B, Lee G-H, Choe H-S, Moon S-H, Kwak D-H, Hong S, and Park K-W, 3-D Si/carbon nanofiber as a binder/current collector-free anode for lithium-ion batteries. *Journal of Industrial and Engineering Chemistry*. 2017. **49**, 105-111

[10] Peng J, Li G, Chen H, Wang D, Jin X, and Chen G Z, Cyclic Voltammetry of ZrO_2 Powder in the Metallic Cavity Electrode in Molten $CaCl_2$. *Journal of The Electrochemical Society*. 2010. **157**, F1-F9

[11] Jiang K, Hu X, Jin X, Wang D, and Chen G Z, Cyclic Voltammetry of Solid TiO_2 in Molten Alkali Chlorides. *ECS Transactions*. 2010. **33 (7)**, 273-276

[12] Ura H, Nishina T, and Uchida I, Electrochemical measurements of single particles of Pd and $LaNi_5$ with a microelectrode technique. *Journal of Electroanalytical Chemistry*. 1995. **396**, 169-173

[13] Z.-X. Dai D-H W, J.-Y. Zou, and Y.-H. Zhouz, A "Green" Route to Prepare Electrodes for Lead-Acid Batteries. *Electrochemical and Solid-State Letters*. 2000. **3 (4)**, 180-182

[14] Minguzzi A, Locatelli C, Lugaresi O, Vertova A, and Rondinini S, Au-based/electrochemically etched cavity-microelectrodes as optimal tool for quantitative analyses on finely dispersed electrode materials: Pt/C, IrO_2-SnO_2 and Ag catalysts. *Electrochimica Acta*. 2013. **114**, 637-642

[15] Minguzzi A, Locatelli C, Cappelletti G, Scavini M, Vertova A, Ghigna P, and Rondinini S, IrO_2-based disperse-phase electrocatalysts: a complementary study by means of the cavity-microelectrode and ex-situ X-ray absorption spectroscopy. *Journal of Physical Chemistry A*. 2012. **116**, 6497-6504

[16] Zou X, Ji L, Lu X, and Zhou Z, Facile electrosynthesis of silicon carbide nanowires from silica/carbon precursors in molten salt. *Sci Rep*. 2017. **7**, 1-9

[17] Cachet-Vivier C, Keddam M, Vivier V, and Yu L T, Development of cavity microelectrode devices and their uses in various research fields. *Journal of Electroanalytical Chemistry*. 2015. **688**, 12-19

[18] Peng J, Deng Y, Wang D, Jin X, and Chen G Z, Cyclic voltammetry of electroactive and insulative compounds in solid state: A revisit of AgCl in aqueous solutions assisted by metallic cavity electrode and chemically modified electrode. *Journal of Electroanalytical Chemistry*. 2009. **627**, 28-40

[19] Qiu G, Ma M, Wang D, Jin X, Hu X, and Chen G Z, Metallic Cavity Electrodes for Investigation of Powders Electrochemical Reduction of NiO and Cr_2O_3 Powders in Molten $CaCl_2$. *Journal of The Electrochemical Society*. 2005. **152（10）**, E328-E336

[20] Morandi S and Minguzzi A, The cavity-microelectrode as a tip for scanning electrochemical microscopy. *Electrochemistry Communications*. 2015. **59**, 100-103

[21] Sze S M and Ng K K, *Physics of Semiconductor Devices*. 2006: Wiley-Interscience.

[22] Jiménez A R, Klöpsch R, Wagner R, Rodehorst U C, Kolek M, Nölle R, Winter M, and Placke T, A Step toward High-Energy Silicon-Based Thin Film Lithium Ion Batteries. *ACS Nano*. 2017. **11**, 4731-4744

[23] Ma Y, Tang H, Zhang Y, Li Z, Zhang X, and Tang Z, Facile synthesis of Si-C nanocomposites with yolk-shell structure as an anode for lithium-ion batteries. *Journal of Alloys and Compounds*. 2017. **704**, 599-606

[24] Weydanz W J, Wohlfahrt-Mehrens M, and Huggins R A, A room temperature study of the binary lithium–silicon and the ternary lithium–chromium–silicon system for use in rechargeable lithium batteries. *Journal of Power Sources*. 1999. **81-82**, 237-242

[25] Zhu J, Guo M, Liu Y, Shi X, Fan F, Gu M, and Yang H, In Situ TEM of Phosphorus-Dopant-Induced Nanopore Formation in Delithiated Silicon Nanowires. *ACS Appl Mater Interfaces*. 2019. **11**, 17313-17320

[26] Domi Y, Usui H, Shimizu M, Kakimoto Y, and Sakaguchi H, Effect of Phosphorus-Doping on Electrochemical Performance of Silicon Negative Electrodes in Lithium-Ion Batteries. *ACS Appl Mater Interfaces*. 2016. **8**, 7125-7132

[27] Tang F, Tan Y, Jiang T, and Zhou Y, Phosphorus-doped silicon nanoparticles as high performance LIB negative electrode. *Journal of Materials Science*. 2022. **57**, 2803-2812

[28] Chao D, Zhu C, Yang P, Xia X, Liu J, Wang J, Fan X, Savilov S V, Lin J, Fan H J, and Shen Z X, Array of nanosheets render ultrafast and high-capacity Na-ion storage by tunable pseudocapacitance. *Nat Commun*. 2016. **7**, 1-8

[29] Wang B, Li X, Luo B, Hao L, Zhou M, Zhang X, Fan Z, and Zhi L, Approaching the downsizing limit of silicon for surface-controlled lithium storage. *Adv Mater*. 2015. **27**, 1526-1532

[30] Brezesinski T, Wang J, Tolbert S H, and Dunn B, Ordered mesoporous alpha-MoO_3 with iso-oriented nanocrystalline walls for thin-film pseudocapacitors. *Nat Mater*. 2010. **9**, 146-51

[31] Liu Y, Qin L, Liu F, Fan Y, Ruan J, and Zhang S, Interpenetrated 3D porous silicon as high stable anode material for Li-Ion battery. *Journal of Power Sources*. 2018. **406**, 167-175

[32] Strauß F, Hüger E, Julin J, Munnik F, and Schmidt H, Lithium Diffusion in Ion-Beam Sputter-Deposited Lithium–Silicon Layers. *The Journal of Physical Chemistry C*. 2020. **124**, 8616-8623

[33] Uxa D, Hüger E, Dörrer L, and Schmidt H, Lithium-Silicon Compounds as Electrode Material for Lithium-Ion Batteries. *Journal of The Electrochemical Society*. 2020. **167**, 130522

[34] Jiang Y and Liu J, Definitions of Pseudocapacitive Materials: A Brief Review. *Energy & Environmental Materials*. 2019. **2**, 30-37

[35] Liu C, Xia Q, Liao C, and Wu S, Pseudocapacitance contribution to three-dimensional micro-sized silicon@Fe_3O_4@few-layered graphene for high-rate and long-life lithium ion batteries. *Materials Today Communications*. 2019. **18**, 66-73

[36] Oloore L E, Gondal M A, Popoola A, and Popoola I K, Pseudocapacitive contributions to enhanced electrochemical energy storage in hybrid perovskite-nickel oxide nanoparticles composites electrodes. *Electrochimica Acta*. 2020. **361**, 137082

[37] Nan Z, Yufan W, Yiran L, Jiankui Y, Qing Z, Yuwei G, Mao X, and Zhi Z, Interconnected structure Si@TiO_2-B/CNTs composite anode applied for high-energy lithium-ion batteries. *Applied Surface Science*. 2020. **500**, 144026.1-9

[38] Wang X, Hao H, Liu J, Huang T, and Yu A, A novel method for preparation of macroposous lithium nickel manganese oxygen as cathode material for lithium ion batteries. *Electrochimica Acta*. 2011. **56**, 4065-4069

[39] Chou S-L, Wang J-Z, Liu H-K, and Dou S-X, Rapid Synthesis of Li4Ti5O12 Microspheres as Anode Materials and Its Binder Effect for Lithium-Ion Battery. *The Journal of Physical Chemistry C*. 2011. **115**, 16220-16227